An EPR study of trigonally symmetric Cr^{3+} centres in $TlZnF_3$ single crystals

2005 J. Phys.: Condens. Matter 17 4653

(http://iopscience.iop.org/0953-8984/17/29/008)

INSTITUTE OF PHYSICS PUBLISHING JOURNAL OF PHYSICS: CONDENSED MATTER

J. Phys.: Condens. Matter **17** (2005) 4653–4663 doi:10.1088/0953-8984/17/29/008

An EPR study of trigonally symmetric Cr^{3+} centres in $TlZnF_3$ single crystals

H Ebisu[1], **M Arakawa**[2] **and H Takeuchi**[3]

[1] Department of Electrical and Electronics Engineering, Nagoya Institute of Technology, Nagoya 466-8555, Japan
[2] Department of Materials Science and Engineering, Nagoya Institute of Technology, Nagoya 466-8555, Japan
[3] Department of Advanced Science and Technology, Toyota Technological Institute, Nagoya 468-8511, Japan

Received 19 May 2005, in final form 24 June 2005
Published 8 July 2005
Online at stacks.iop.org/JPhysCM/17/4653

Abstract

EPR measurements have been made on the single crystals of $TlZnF_3$ doped with chromium and co-doped with chromium and lithium. For the Cr-only doped crystal, three kinds of Cr^{3+} spectra with trigonal symmetry were observed. These centres are ascribed respectively to a charge-uncompensated Cr^{3+} ion at the Zn_2F_9 unit (Zn site II), a Cr^{3+} ion associated with a nearest Zn^{2+} vacancy at the Zn_2F_9 unit, and a charge-uncompensated Cr^{3+} ion at the ZnF_6 unit (Zn site I). In the Cr, Li co-doped crystal, preferential formation of a Cr^{3+}–Li^+ pair at the Zn_2F_9 unit was found. The ligand octahedra are considered to be elongated in the Cr^{3+}–Zn^{2+} and the Cr^{3+}–Li^+ centres at the Zn_2F_9 units and compressed in the Cr^{3+} centre at the ZnF_6 unit.

1. Introduction

The structure of an ABF_3 crystal at room temperature is characterized by the tolerance factor $t = (r_A + r_F)/[\sqrt{2}(r_B + r_F)]$, where r_A, r_B and r_F are respectively the ionic radii of the A^+, B^{2+} and F^- ions. The tolerance factors of $RbZnF_3$ and $TlZnF_3$ are close to the boundary of the cubic perovskite structure ($t \simeq 0.88$–1.00) and the hexagonal-$BaTiO_3$ type structure with the space group $P6_3/mmc$ ($t \simeq 1.00$–1.06) [1, 2]. In fact, upon cooling a pure crystal of $RbZnF_3$, its structure changes from the hexagonal-$BaTiO_3$ type structure (h-$RbZnF_3$) to the cubic perovskite structure (c-$RbZnF_3$) at about 640 °C [3]. Moreover, it was found in the previous work [4] that some $RbZnF_3$ crystal co-doped with chromium and lithium has the hexagonal structure even at 4.2 K. On the other hand, the $TlZnF_3$ crystal has the hexagonal-$BaTiO_3$ type structure until 4.2 K without any structural phase transitions on lowering temperature from the melting point.

The crystal structure of $TlZnF_3$ is shown in figure 1. The structure has two kinds of Zn sites. One Zn site is in a ZnF_6 unit of a single octahedron (called Zn site I). The fluorine

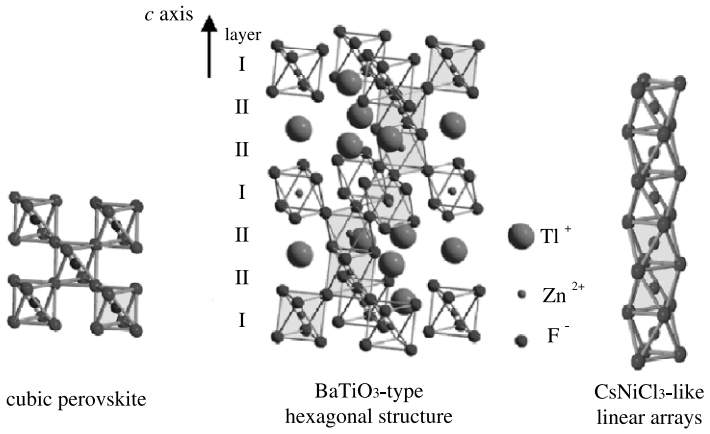

Figure 1. The hexagonal-$BaTiO_3$ type structure of the $TlZnF_3$ crystal and the arrays of anion octahedra in the $KNiF_3$-like cubic perovskite structure and the $CsNiCl_3$-like hexagonal structure. The layers of Zn sites I and II normal to the crystalline *c* axis are marked with I or II, respectively.

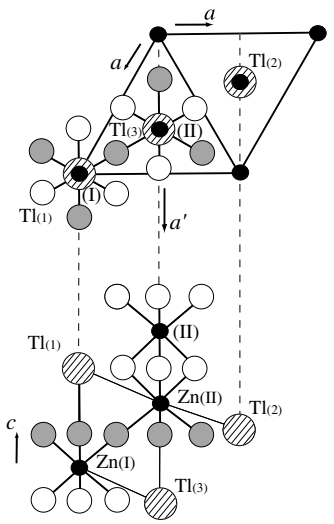

Figure 2. The local environments of the substitutional Zn sites I and II for magnetic ions doped in $TlZnF_3$ crystal. Open and shaded circles of medium size are F^- ions, where the shaded circles are in the same layer. The marks $Tl_{(1)}$, $Tl_{(2)}$ and $Tl_{(3)}$ denote the different types of Tl^+ ions relative to Zn sites I and II. The upper part shows the projection of the Zn sites and surroundings into the *c* plane. *a* and *a*′ denote the directions in the *c* plane.

octahedron surrounding Zn site I is linked to six other octahedra at the six corners similarly to the perovskite crystals. The other Zn site is in a Zn_2F_9 unit composed of two face-sharing octahedra (called Zn site II). In contrast with Zn site I, the fluorine octahedron surrounding Zn site II is linked to three other octahedra at the three ligands similarly to the perovskite crystals and to one face-sharing octahedron at the other three ligands similarly to the $CsNiCl_3$-like crystals having linear arrays of face-sharing octahedra [5, 6]. Figure 2 shows the local environments of the substitutional Zn sites I and II in the $TlZnF_3$ crystal. The shaded circles of medium size are F^- ions in the *c* plane common to the octahedra of sites I and II. Three

types of Tl^+ ions in the neighbourhood of the Zn^{2+} ions are shown by $Tl_{(1)}$, $Tl_{(2)}$ and $Tl_{(3)}$. The upper part of the figure shows the projection of Zn sites I and II and their surroundings into the c plane. a and a' denote the axis directions in the c plane.

It is interesting to investigate what kinds of magnetic impurity centres are formed in the hexagonal-$BaTiO_3$ type crystal in comparison with the formation of the magnetic impurity centres in perovskite crystals and $CsNiCl_3$-like crystals. The electron paramagnetic resonance (EPR) experiment is useful for obtaining information on the local environments for the magnetic impurity ions doped in ionic crystals. In this paper, we will report results of the EPR experiments for $TlZnF_3$ crystals doped only with chromium and co-doped with chromium and lithium. In the previous EPR result for the Cr^{3+} centres in $CsMgCl_3$ crystals [6], the relationship between the fine structure parameter b_2^0 and the distortion of the ligand octahedron was studied in the series of several trigonal Cr^{3+} centres formed in the same host crystal. The crystal of $TlZnF_3$ may also be valuable as a matrix to investigate the above relationship in the series of Cr^{3+} centres formed in the same host crystal. So, we focus our attention on the Cr^{3+} centres with trigonal symmetry about the crystalline c axis. We expect to clarify the characteristics in the local environment of the centres formed at Zn sites I and II and their differences.

In the EPR measurements for the Cr-only doped crystal, three kinds of Cr^{3+} spectra having trigonal symmetry were observed. From the Cr, Li co-doped crystal, another Cr^{3+} spectrum having trigonal symmetry was observed. The spin-Hamiltonian parameters for the spectra will be determined from their angular variations using a direct matrix-diagonalization method and from the knowledge of the depopulation effects observed at the low temperature of 4.2 K. To ensure the identifications of the impurity centres, the change of EPR spectra by x-ray irradiation was examined. From the experimental results, each spectrum will be ascribed to a respective Cr^{3+} ion substituting for a Zn^{2+} ion. The fine structure parameters b_2^0 obtained for the centres formed in Zn sites I and II will be discussed in relation to the distortion of the ligand octahedron and be compared with those for the trigonal Cr^{3+} centres in $CsMgCl_3$ and h-$RbZnF_3$.

2. Experimental procedures

Single crystals of $TlZnF_3$ doped with chromium were grown in the glassy carbon crucibles using the Bridgman technique. As the magnetic impurity, powdered CrF_3 of 0.3 mol% was added to the starting mixture of powdered TlF and ZnF_2. For some starting mixtures, LiF powder of about 0.1 mol% was added. The glassy carbon crucible was heated to 450 °C in argon atmosphere to yield liquid mixtures. Then, the temperature was lowered for crystallization with a cooling rate of 50 °C h^{-1}. Obtained crystals have pale yellow–greenish colour. EPR measurements were made at room temperature and 4.2 K using a JES-FE1XG X-band spectrometer with 100 kHz field modulation at the Advanced Instrument and Analysis Division in Nagoya Institute of Technology. Single crystals having natural planes were used in the measurements. An NMR probe EFM-2000 (Echo Electronics) was used for accurate measurement of external magnetic field. Parameter fitting of the spin Hamiltonians was performed by a direct matrix-diagonalization method. The depopulation effect was observed at 4.2 K using X-band microwave for the determination of the signs of the b_2^0 parameters.

3. Results

EPR measurements were carried out for the Cr-only doped crystal and the Cr, Li co-doped crystal. Figure 3(a) shows a recorder trace of the EPR spectrum observed for the Cr-only doped crystal at room temperature with $\boldsymbol{H} \parallel c$ axis. Several signals to be ascribed to some Cr^{3+} centres were observed. The signals are marked with A, B or C to distinguish different

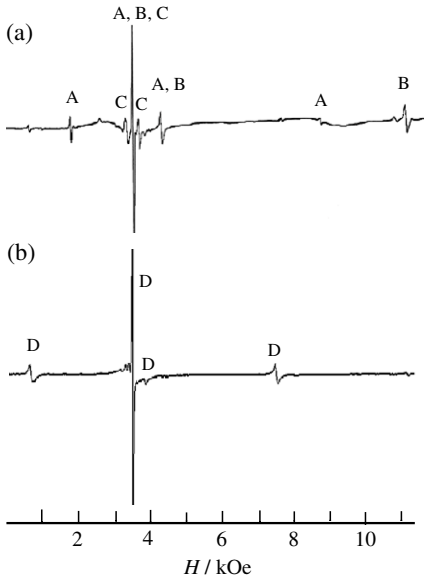

Figure 3. EPR spectra observed at 297 K with $\boldsymbol{H} \parallel c$ axis using the X-band spectrometer. Signals from the as-grown crystals of $TlZnF_3$ (a) doped with only Cr and (b) co-doped with Cr and Li. The signals are marked with A, B, C or D to distinguish different types of magnetic impurity centre.

types of magnetic impurity centres to be identified later. The relative intensity among the signals A, B and C changed for different samples cleaved from the same batch of the Cr-only doped crystal.

Figure 3(b) shows a recorder trace of the EPR spectrum observed from the Cr, Li co-doped crystal. New EPR signals marked with D were observed. The intensity of the signals D was superior to the intensity of other signals. Signals A, B and C were not observed distinctly in the Cr, Li co-doped crystal.

Figure 4 shows the angular variations of the signals A, B and C marked in figure 3(a) when the external field is rotated from $\boldsymbol{H} \parallel c$ to $\boldsymbol{H} \perp c$ axis directions. For each type of the signals, the angular variation shows maximum fine structure splitting when the external field is parallel to the c axis direction. Moreover, the resonant fields were unchanged by the rotation of the external field in the c plane. The above results show that the spectra for signals A, B and C have axial symmetry about the c axis. Figure 5 shows the angular variation of signals D observed from the Cr, Li co-doped crystal. The spectrum showed axial symmetry about the c axis. The features of the spectra show clearly that signals A, B, C and D can be ascribed to the Cr^{3+} ions situated respectively in different types of local environment having trigonal symmetry about the c axis. Hereafter, these centres are called trigonal Cr^{3+} centres A, B, C and D.

The spectra of the trigonal Cr^{3+} centres can be described by the following spin Hamiltonian with $S = \frac{3}{2}$;

$$\mathcal{H} = g_{\parallel}\beta S_z H_z + g_{\perp}\beta(S_x H_x + S_y H_y) + \tfrac{1}{3}b_2^0 O_2^0, \tag{1}$$

where $g_{\parallel} \equiv g_z$, $g_{\perp} \equiv g_x = g_y$ and O_2^0 is the Stevens operator given by Abragam and Bleaney [7]. The main principal axis (z axis) is parallel to the crystalline c axis.

For the determination of the absolute signs of b_2^0 for centres A, B and D, we examined the depopulation effect at 4.2 K in the $\boldsymbol{H} \perp c$ axis direction. Figure 6 shows the recorder trace

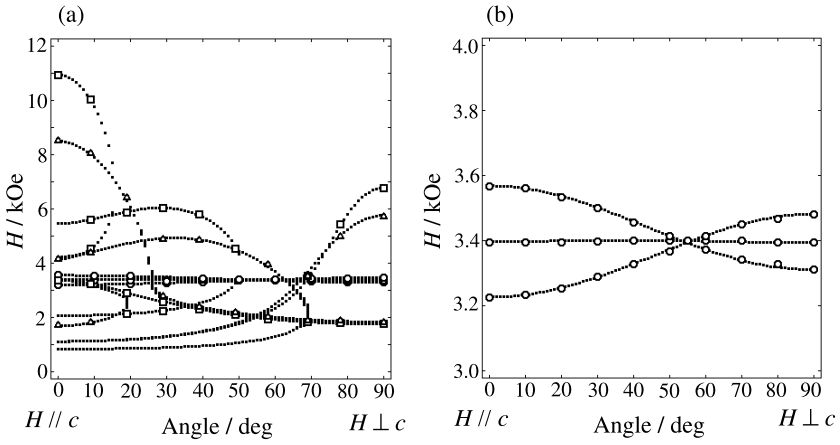

Figure 4. Angular variations of signals A, B and C. (a) Triangles, squares and circles represent respectively the variations of experimental resonant fields for the signals A, B and C shown in figure 3(a). Dotted curves indicate theoretical resonant values computed using the spin-Hamiltonian parameters listed in table 1. (b) The magnified angular variations of signals C around 3.4 kOe.

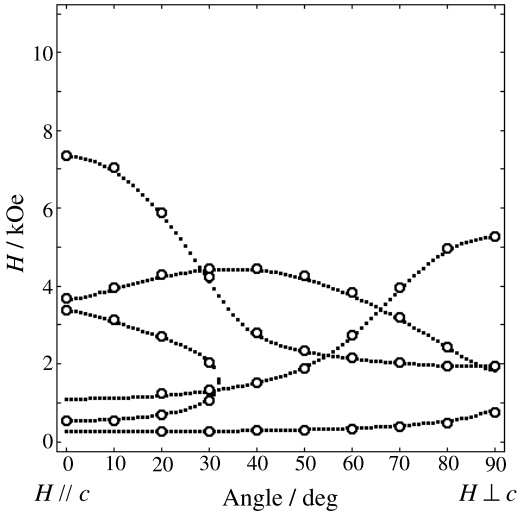

Figure 5. Angular variations of signals D. Circles represent the variations of experimental resonant fields for the signals D shown in figure 3(b). Dotted curves indicate theoretical resonant values computed using the spin-Hamiltonian parameters listed in table 1.

of the observed spectrum. For the EPR transitions $\pm\frac{3}{2} \leftrightarrow \pm\frac{1}{2}$, the ratio of the intensity I_H of the high-field signal to the intensity I_L of the low-field signal at 4.2 K was compared with that obtained at room temperature. For centre A, the ratio I_H/I_L at 4.2 K increased from that at the room temperature. On the other hand, for centre B, the ratio at 4.2 K decreased from that at room temperature. In the $\boldsymbol{H} \perp c$ axis direction, increase of the relative intensity I_H/I_L at low temperature from the value at room temperature indicates a negative sign of b_2^0 and decrease indicates a positive sign of b_2^0, inversely to the situation with $\boldsymbol{H} \parallel c$. Thus, the above experimental results show that the absolute signs of b_2^0 are negative for centre A and positive for centre B. The sign of b_2^0 for centre D was determined to be positive by a similar analysis

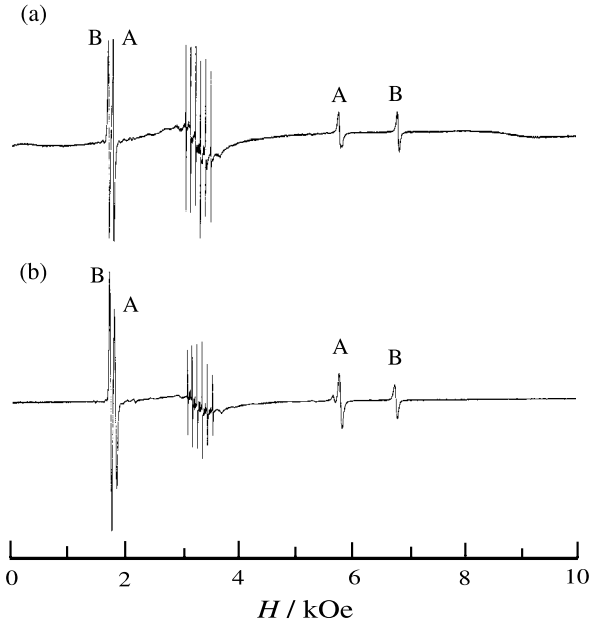

Figure 6. EPR spectra with $\boldsymbol{H} \perp c$ observed at (a) 297 K and (b) 4.2 K from $TlZnF_3$ doped with only Cr. The roman capitals A and B denote respectively the signals from centres A and B in figure 3(a). The six-line hyperfine signals around 3.4 kOe are reference signals from $MgO:Mn^{2+}$.

Table 1. Spin-Hamiltonian parameters obtained at 297 K for several kinds of trigonal Cr^{3+} centres in $TlZnF_3$. Units are in 10^{-4} cm^{-1} for b_2^0.

Centre	$g_\parallel$	$g_\perp$	b_2^0	$g_\parallel - g_\perp$
A	1.9692(2)	1.9708(2)	−2387.0(2)	−0.0016
B	1.9750(2)	1.9727(2)	+3496.9(2)	+0.0023
C	1.9723(2)	1.9730(2)	−78.8(3)	−0.0007
D	1.9774(2)	1.9738(2)	+1849.3(2)	+0.0036

of the depopulation effect at 4.2 K. The spin-Hamiltonian parameters obtained by the matrix-diagonalization method are listed in table 1. For centre C, the sign of b_2^0 was not determined by the observation of depopulation effect since the fine structure splitting disappeared below 77 K. For each centre A, B and D, the axial fine structure parameter b_2^0 and the axiality of the g tensor $g_\parallel - g_\perp$ have the same signs, similarly to the case of the trigonal Cr^{3+} centres in the perovskite fluorides. So, it may be reasonable to consider that the sign of b_2^0 for centre C is negative to be the same as $g_\parallel - g_\perp$.

The samples of the Cr-only doped crystal and the Cr, Li co-doped crystal were x-ray irradiated at room temperature for 3 h in a dark environment using a Cu tube operating at 40 kV and 30 mA. Figure 7(b) shows the recorder trace of the EPR spectrum observed after x-ray irradiation for a Cr-only doped crystal whose EPR spectrum before irradiation is shown in figure 7(a). The EPR signals of centres A and B were enhanced after x-ray irradiation. The degree of the enhancement by the irradiation was different for each sample crystal. The signal intensity of centre C was not changed by the irradiation. As for the Cr, Li co-doped crystal, distinct change of the spectra was not observed with the x-ray irradiation, in contrast with the case of the Cr-only doped crystal.

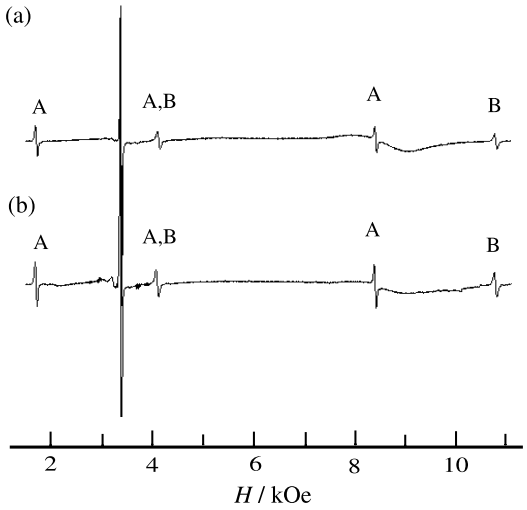

Figure 7. EPR spectra with $\boldsymbol{H} \parallel c$ observed at room temperature from a Cr-only doped $TlZnF_3$ (a) before x-ray irradiation and (b) after x-ray irradiation.

4. Discussion

4.1. Trigonal centres A and B

Davies and Horai [8] reported in their EPR and ENDOR studies on the Cr centres formed in $KMgF_3$ that the signal intensity of the cubic Cr^{3+} centre was enhanced and new cubic Cr^{+} signals appeared after x-ray irradiation of the sample crystal. They explained the phenomena as follows: the x-ray scatters the electrons of some Cr^{2+} ions at the host Mg^{2+} sites and some of the scattered electrons were caught by other Cr^{2+} ions. As a result, the Cr^{2+} ion whose electron was scattered changes to a Cr^{3+} ion and the Cr^{2+} ion which has caught one electron changes to a Cr^{+} ion.

For some $TlZnF_3$ crystals doped only with chromium, the enhancement of the signal intensity of centres A and B was observed after x-ray irradiation as seen from figure 7. Similarly to the case of $KMgF_3$, we may say for the present crystal of $TlZnF_3$ that in crystallization some of the chromiums substitute for the Zn^{2+} ions in the Cr^{2+} state without charge misfit and some of them are changed into Cr^{3+} ions by the x-ray irradiation, although no distinct signals of Cr^{+} were observed. So, centres A and B may be ascribed to the charge-uncompensated Cr^{3+} ions at either the Zn sites I or II, where the Cr^{3+} ions are not associated with any charge compensators in their immediate neighbourhood.

Next, we examine which Zn sites (I or II) are corresponding to centres A and B. As for the crystal structure, detailed values of bond lengths and bond angles are reported for $CsMnF_3$ [9] which is isomorphous to $TlZnF_3$. The ratio of the lattice parameter c/a (=2.45) for $TlZnF_3$ [1] is almost the same as the value of $CsMnF_3$ (2.43), although the lattice parameter a (=5.934 Å) for $TlZnF_3$ is a little smaller than 6.213 Å for $CsMnF_3$. So, the deformations of the ligand octahedra for Zn sites I and II in $TlZnF_3$ may be similar to those for the Mn sites in $CsMnF_3$ except for the smaller metal–ligand distances for $TlZnF_3$. In $CsMnF_3$, the Mn–F distance and the F–Mn–F angle are (2.098 Å, 94.3°) for the fluorine octahedron of the single unit MnF_6 with inversion symmetry (Mn site I). This shows that the fluorine octahedron of site I is compressed along the crystalline c axis from the regular octahedral configuration. On the

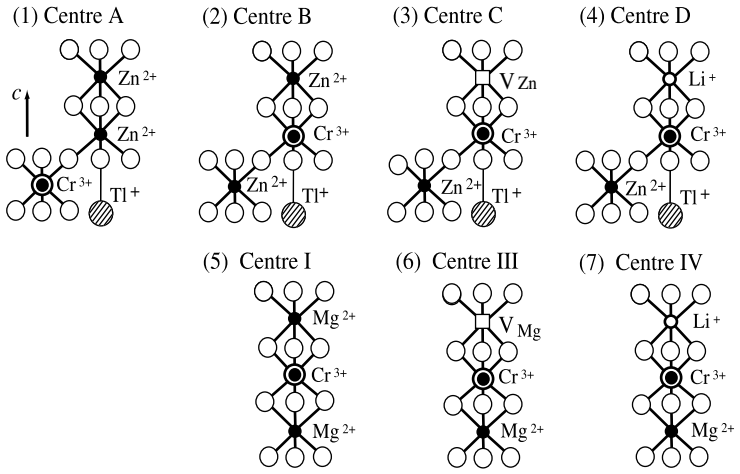

Figure 8. Schematic models for the four trigonal Cr^{3+} centres A, B, C and D formed in the $TlZnF_3$ crystals are shown respectively as (1) Cr^{3+}(I), (2) Cr^{3+}–Zn^{2+}, (3) Cr^{3+}–V_{Zn} and (4) Cr^{3+}–Li^{+} centres. The trigonal Cr^{3+} centres I, III and IV formed in the $CsMgCl_3$ crystals are also shown as (5) Cr^{3+}–Mg^{2+}, (6) Cr^{3+}–V_{Mg} and (7) Cr^{3+}–Li^{+} centres for comparison.

other hand, the fluorine octahedron of the double unit Mn_2F_9 has a small and a large regular triangle face parallel to the c plane and so does not have inversion symmetry (Mn site II). For the asymmetric fluorine octahedron of site II, the two sets of Mn–F distances and F–Mn–F angles are (2.164 Å, 77.1°) for the F^- ions in the small triangle face intervening between two Mn^{2+} ions and (2.113 Å, 95.9°) for the F^- ions in the large triangle face. The former angle corresponds to an elongation of the octahedron and the latter to compression. However, the ligand octahedron may be considered as elongated effectively since the deviation of the former angle from the regular value (90°) is much larger than the deviation of the latter.

McGarvey [10] has presented the theory that a negative b_2^0 value in the centre of a $3d^3$ ion with trigonal symmetry arises from the d electrons being more concentrated along the trigonal axis by the compression of the ligand octahedron along the axis. Later, Danilov and Manoogian [11, 12] found a rule by means of the EPR and ENDOR experiments that the positive and negative values of the b_2^0 parameter for the trigonal Cr^{3+} centres correspond respectively to elongation and compression of the ligand octahedron along the trigonal axis. From the empirical rule, centre A with the negative b_2^0 value is considered to have a compressed ligand octahedron, and centre B with the large positive b_2^0 value is considered to have an elongated ligand octahedron. Thus, centre A can be ascribed to a Cr^{3+} ion substituting for the Zn^{2+} ion at site I without any charge compensator in its immediate neighbourhood (Cr^{3+}(I) centre), and centre B can be ascribed to a Cr^{3+} ion substituting for the Zn^{2+} ion at site II without any charge compensator in its immediate neighbourhood (Cr^{3+}–Zn^{2+} centre). The schematic models for these centres are shown in figures 8(1) and (2).

The elongation of the ligand octahedron for centre B may be caused by the increased cation–cation repulsion for the Cr^{3+} ion substituting for the Zn^{2+} ion at site II. The magnitude of b_2^0 for centre A is considerably larger than those for the trigonal Cr^{3+}–V_K centres in $KZnF_3$ ($-1613 \times 10^{-4}\,cm^{-1}$) and $KMgF_3$ ($-1528 \times 10^{-4}\,cm^{-1}$) [13], where the ligand octahedra are compressed along the trigonal axis due to the K^+ vacancy. As the ionic radius of a Cr^{3+} ion is smaller than that of a Zn^{2+} ion, the fluorine octahedron surrounding the Cr^{3+} ion of centre A may be compressed strongly along the c axis by the tendency of elongation of six Zn_2F_9 units sharing corners with the CrF_6 unit.

Table 2. Comparison of the values of b_2^0 for the trigonal Cr^{3+} centres observed in $TlZnF_3$ with the b_2^0 values of the Cr^{3+} centres observed in $CsMgCl_3$ and h-$RbZnF_3$ crystals. Units are 10^{-4} cm^{-1}.

$TlZnF_3$		$CsMgCl_3$		$RbZnF_3$	
This work	b_2^0	[6]	b_2^0	[4]	b_2^0
B: Cr^{3+}–Zn^{2+}	3496.9	Cr^{3+}–Mg^{2+}	1253.3	—	—
D: Cr^{3+}–Li^{+}	1849.3	Cr^{3+}–Li^{+}	−86.6	Cr^{3+}–Li^{+}	1597.3
C: Cr^{3+}–V_{Zn}	−78.8	Cr^{3+}–V_{Mg}	−2811.8	—	—
A: Cr^{3+} (I)	−2387.0	—	—	—	—

It is considered from the above empirical rule that the positive value of b_2^0 for the uncompensated centre (centre I in figure 8(5)) in $CsMgCl_3$ [6] shows the elongated face-sharing ligand octahedron along the trigonal c axis due to the electronic repulsion between the Cr^{3+} ion and the neighbouring Mg^{2+} ions. On the other hand, the negative value of b_2^0 for the Cr^{3+}–Li^{+} centre (centre IV in figure 8(7)) suggests that the ligand octahedron changes to a compressed one since the cation–cation repulsion is decreased due to a monovalent deficient charge on the Li^{+} ion at the Mg^{2+} site. Moreover, in the Cr^{3+}–V_{Mg} centre (centre III in figure 8(6)), the value of b_2^0 is negative with large magnitude due to a divalent deficient charge on the Mg^{2+} vacancy, showing that the ligand octahedron is further compressed from that of the Cr^{3+}–Li^{+} centre. Thus, the difference of the b_2^0 values among the three kinds of trigonal Cr^{3+} centres formed respectively in the face-sharing octahedra of $TlZnF_3$ and $CsMgCl_3$ can be understood by the differences in the trigonal distortions of the ligand octahedra.

4.2. Trigonal centre D

The trigonal centre D was formed only in the Cr, Li co-doped crystal. The signals of centre D are superior to other signals as seen from figure 2. For the co-doped crystal, a distinct change of the spectrum by the x-ray irradiation was not observed. That is, the enhanced signals of centres A and B were not observed distinctly after the x-ray irradiation. So, in the co-doped crystal, the Zn^{2+} ions are considered not to be substituted by Cr^{2+} ions in contrast with the case of the Cr-only doped crystal. Centre D is found to be formed preferentially. This suggests that a Cr^{3+} ion in this centre is associated with a Li^{+} ion nearby on the c axis as a charge compensator. From the above features, centre D can be ascribed to a Cr^{3+} ion at Zn site II associated with a Li^{+} ion at the adjacent Zn site II on the c axis for charge compensation. The centre is shown in figure 8(4). The preferential formation of this Cr^{3+}–Li^{+} centre may be understood by its advantage of just charge compensation to other types of Cr^{3+} centres and smaller cation–cation repulsion than the Zn^{2+}–Zn^{2+} pair.

In table 2, the b_2^0 parameters of the trigonal centres in $TlZnF_3$ are compared with the b_2^0 parameters of the Cr^{3+} centres in $CsMgCl_3$ and h-$RbZnF_3$ crystals. The value of b_2^0 for centre D is comparable with the b_2^0 value for the trigonal Cr^{3+} centre in the isomorphous hexagonal $RbZnF_3$ crystal. It is confirmed from this fact that the trigonal centre observed in the hexagonal $RbZnF_3$ is the Cr^{3+}–Li^{+} centre formed at Zn site II. This shows that the Cr^{3+}–Li^{+} centre is formed preferentially in crystallization of $RbZnF_3$ and is stable in the hexagonal phase, which is found to exist even at the low temperature of 4.2 K below the transition temperature 640 °C [4].

As the electrostatic repulsion between Cr^{3+} and Li^{+} is weaker than the repulsion between Cr^{3+} and Zn^{2+}, the elongation of the fluorine octahedron surrounding the Cr^{3+} ion is expected to be smaller in the Cr^{3+}–Li^{+} centre (centre D) than that in the Cr^{3+}–Zn^{2+} centre (centre B). In fact, the axial parameter b_2^0 for the Cr^{3+}–Li^{+} centre decreased by 1648×10^{-4} cm^{-1} from

the value of the Cr^{3+}–Zn^{2+} centre. This situation is similar to the decrease in b_2^0 of the Cr^{3+} centre in $CsMgCl_3$, where b_2^0 of the Cr^{3+}–Li^+ centre decreased by 1340×10^{-4} cm^{-1} from the value of the Cr^{3+}–Mg^{2+} centre. The hexagonal-$BaTiO_3$ type structure is considered to become unstable with increasing cation–cation repulsion in the double octahedron unit and tends to change to the perovskite structure. The formation of the Cr^{3+}–Li^+ centre in the high temperature hexagonal phase may weaken the tendency to change the hexagonal structure.

4.3. Trigonal centre C

The signal intensity of the trigonal centre C was not changed distinctly by x-ray irradiation. That is, there may be no Cr^{2+} ions to be changed to the Cr^{3+} ions of this centre by x-ray irradiation. This suggests that the Cr^{3+} ion of centre C is associated with some charge compensator along the *c* axis direction. Moreover, the trigonal centre C has very small magnitude of the b_2^0 value. It is found from above facts that the configuration of the ligand octahedron in centre C is close to a regular octahedral configuration in spite of the association of a charge compensator on the *c* axis.

The Cr^{3+} ion substituting for a Zn^{2+} ion at site I with an association of the $Tl^+_{(1)}$ ion vacancy on the trigonal axis is discarded as centre C since the Cr^{3+}(I)–$V_{Tl(1)}$ centre should have a more compressed ligand octahedron than that of centre A. On the other hand, if the Cr^{3+} ion substituting for a Zn^{2+} ion at site II is associated with the Zn^{2+} vacancy at the adjacent Zn site II on the *c* axis, the cation–cation repulsion for the Cr^{3+} ion vanishes. As a result the ligand octahedron may become close to a regular octahedron, so that the magnitude of the b_2^0 parameter for the centre is expected to be considerably smaller than that for the Cr^{3+}–Li^+ centre. From the above discussions, centre C may be ascribed to a Cr^{3+} ion at site II associated with a Zn^{2+} vacancy (Cr^{3+}–V_{Zn} centre). The schematic model of the centre is shown in figure 8(3).

The axial parameter b_2^0 for the Cr^{3+}–V_{Zn} centre decreased by 3576×10^{-4} cm^{-1} from the b_2^0 value of the Cr^{3+}–Zn^{2+} centre. As seen from table 2, this decrease is comparable with that in the Cr^{3+} centres in $CsMgCl_3$, where b_2^0 of the Cr^{3+}–V_{Mg} centre decreased by 4065×10^{-4} cm^{-1} from the value of the Cr^{3+}–Mg^{2+} centre. The absolute values of b_2^0 for both Cr^{3+}–V_M centres are considerably different to each other although the decreases of b_2^0 from the values for the charge-uncompensated centres are comparable. This may be related to the fact that the Cr^{3+}–Mg^{2+} repulsion on the other side of the Mg^{2+} vacancy is left for the Cr^{3+}–V_{Mg} centre in $CsMgCl_3$ in contrast with the case of the Cr^{3+}–V_{Zn} centre in the $TlZnF_3$ crystal.

5. Conclusions

From the Cr-only doped crystal of $TlZnF_3$, three kinds of Cr^{3+} centres having trigonal symmetry about the crystalline *c* axis were observed. These trigonal centres are identified respectively as the Cr^{3+} centre at a Zn site II in the Zn_2F_9 unit associated with a Zn^{2+} vacancy at the adjacent site on the *c* axis (Cr^{3+}–V_{Zn} centre), the charge-uncompensated Cr^{3+} centre at a Zn site I in the ZnF_6 unit (Cr^{3+}(I) centre), and the charge-uncompensated Cr^{3+} centre at a Zn site II (Cr^{3+}–Zn^{2+} centre). The intensity of the EPR signals from the charge-uncompensated Cr^{3+} centres was enhanced after x-ray irradiation for the Cr-only doped crystal. The result shows that some of the chromiums doped in the crystal exist in the Cr^{2+} state and change into the Cr^{3+} state by x-ray irradiation.

The Cr^{3+} centre observed newly from the sample co-doped with Cr and Li is identified to be the Cr^{3+} centre formed at a Zn site II associated with a Li^+ ion at the adjacent Zn site II (Cr^{3+}–Li^+ centre). Preferential formation of the Cr^{3+}–Li^+ centre was observed. In the Cr, Li co-doped crystal, the signal intensity of this centre is superior to other trigonal Cr^{3+} centres,

and chromiums may not exist in the Cr^{2+} state in contrast with the case in the Cr-only doped crystal. It is considered that the Cr^{3+}–Li^{+} centre has advantages of just charge compensation and small cation–cation repulsion to other centres in the formation of the magnetic impurity centres.

The large positive b_2^0 value for the Cr^{3+}–Zn^{2+} centre at Zn site II is understood by the elongation of the octahedron surrounding the Cr^{3+} ion due to the increased cation–cation repulsion between the Cr^{3+} and the Zn^{2+} ions. The ligand octahedron surrounding the Cr^{3+} ion in the Cr^{3+}–Li^{+} centre is considered also to be elongated due to the Cr^{3+}–Li^{+} repulsion. On the other hand, the ligand octahedron surrounding the Cr^{3+} ion in the Cr^{3+}–V_{Zn} centre is considered to be close to regular octahedral configuration due to absence of the cation–cation repulsion. The decrease of the axial b_2^0 parameter in the series of the trigonal Cr^{3+} centres in $TlZnF_3$ is comparable to the decrease of b_2^0 in the series of the Cr^{3+} centres in $CsMgCl_3$. In contrast with the trigonal Cr^{3+} centres formed in the Zn_2F_9 unit, the charge-uncompensated Cr^{3+} centre formed in the ZnF_6 unit has negative b_2^0 value with considerably large magnitude. The ligand octahedron of the centre may be compressed strongly by the tendency of elongation of six Zn_2F_9 units sharing corners with the CrF_6 unit.

References

[1] Babel D 1967 *Struct. Bonding* **3** 1–87
[2] Babel D 1969 *Z. Anorg. Chem.* **369** 117–30
[3] Daniel Ph, Toulouse J, Gesland J Y and Rousseau M 1995 *Phys. Rev.* B **52** 9129–32
[4] Arakawa M, Ebisu H, Takeuchi H and Mori M 1998 Modern applications of EPR/ESR *Proc. 1st Asia-Pacific EPR/ESR Symp.* (Singapore: Springer) pp 445–52
[5] McPherson G L and Devaney K 1980 *J. Phys. C: Solid State Phys.* **13** 1735–43
[6] Takeuchi H, Tanaka H and Arakawa M 1993 *J. Phys.: Condens. Matter* **5** 9205–14
[7] Abragam A and Bleaney B 1970 *Electron Paramagnetic Resonance of Transition Ions* (Oxford: Clarendon)
[8] Davies J J and Horai K 1971 *J. Phys. C: Solid State Phys.* **4** 671–81
[9] Zalkin A, Lee K and Templeton D H 1962 *J. Chem. Phys.* **37** 697–99
[10] McGarvey B R 1964 *J. Chem. Phys.* **40** 809–12
[11] Danilov A G and Manoogian A 1972 *Phys. Rev.* B **6** 4097–103
[12] Danilov A G and Manoogian A 1972 *Phys. Rev.* B **6** 4103–11
[13] Patel J L, Davies J J, Cavenette B, Takeuchi H and Horai K 1976 *J. Phys. C: Solid State Phys.* **9** 129–38